X-ray redshifts with the International X-ray Observatory (IXO)

N. Castelló-Mor * X. Barcons and L. Ballo

Instituto de Física de Cantabria (CSIC-UC), 39005 Santander, Spain

Abstract

We explore the capabilities of the future space science mission IXO (International X-ray Observatory) for obtaining cosmological redshifts of distant AGN (Active Galactic Nuclei) using the X-ray data only. We first find in which regions of the X-ray luminosity (L_X) versus redshift (z) plane the weak but ubiquitous Fe Kα narrow emission line can deliver an accurate redshift ($\delta z < 5\%$) as a function of exposure time, using a CCD-based Wide Field Imager (IXO/WFI) as the one baselined for IXO. Down to a $2-10$ keV X-ray flux of 10^{-14} erg cm^{-2} s^{-1} IXO/WFI exposures of 100 ks, 300 ks and 1 Ms will deliver 20%, 40% and 60% of the redshifts. This means that in a typical $18^{'} \times 18^{'}$ IXO/WFI field of view, 4, 10 and 25 redshifts will be obtained for free from the X-ray data alone, spanning a wide range up to $z \sim 2-3$ and fairly sampling the real distribution. Measuring redshifts of fainter sources will indeed need spectroscopy at other wavebands.

Key words:

1 Introduction

Active galactic nuclei (AGNs) are the most energetic stable phenomena in the Universe, being observable to very large distances. The accretion paradigm states that most, and perhaps all, AGN are powered by accretion onto a supermassive black hole (Blandford & Rees 1991, SMBH). Moreover, the large majority of the energy density generated by accretion onto massive black holes seems to take place in obscured AGN, as demonstrated by the integrated energy density of the cosmic X-ray background (see, e.g. Comastri et al. 1995;

* castello@ifca.unican.es
Email addresses: barcons@ifca.unican.es, ballo@ifca.unican.es (X. Barcons and L. Ballo).

Gilli et al. 2007). The number of obscured AGN decreases with increasing X-ray luminosity in X-ray selected samples of AGN. The current data support the idea that the AGN activity in galaxies is in fact a transition phase in the galaxy formation and many of the galaxies which today do not show this activity could have gone through it in the past (see e.g. Hopkins et al. 2006). **Probably all galaxies have a SMBH at their centre (Magorrian et al. 1998). Black hole mass correlates strongly with the velocity dispersion of the galactic bulge (Gebhardt et al. 2000) and the bulge mass, indicating that the process of SMBH growth and galaxy formation are interlinked. The space density of the brightest AGN peaks around $z \sim 2-2.5$, whereas the one for the less luminous AGN peaks at $z \sim 1$ (Ueda et al. 2003; Hasinger et al. 2005; La Franca et al. 2005)**.

The IXO (International X-ray Observatory) mission [1] will identify active galaxies and quasars in the earliest epochs of the Universe through the radiation from AGN as a result of mass accretion by a super-massive black hole (SMBH) at the centre of the galaxy. Detailed identification of weak X-ray sources usually proceeds through the identification of one or more candidate counterparts in the optical or infrared, followed by spectroscopy at these wavelengths. **Efficient optical spectrometers on $8-10$ meter class telescopes reach an ultimate sensitivity limit for optical spectroscopic identifications at an optical magnitude around $R \sim 24$. Using multi-object spectrometers, redshifts for virtually all X-ray source counterparts brighter than this optical magnitude could be obtained with a few nights of observation in a ground-based state of the art spectrometer on $8-10$ meter class telescope. This corresponds, on average, to X-ray sources with a $2-10$ keV flux of around $10^{-15}\,\mathrm{erg\,cm^{-2}\,s^{-1}}$. However, the X-ray to optical flux ratio (X/O) has a large dispersion, and the high X/O ratio sources are typically difficult to identify. It is for this kind of sources that the method proposed here could save significant optical observing telescope time.**

In this paper, we explore the possibility to use the Fe Kα emission line, observed in all AGN-type sources, as an indicator of the cosmological redshift. **This line has already been used to compute redshifts for galaxy clusters (Hashimoto et al. 2004) and gamma-ray bursts (see e.g. Antonelli et al. 2001). Also, it has been used before to derive the redshifts for few AGN (see e.g. Civano et al. 2005).** This method, *using the X-ray data themselves*, will constitute an important step forward. The detection of iron emission line in AGN-type objects, after accounting for the underlying X-ray continuum, allows us to obtain a unique and distinctive spectroscopic feature generated by the X-ray irradiation from the central AGN

[1] See `http://ixo.gsfc.nasa.gov` and `http://sci.esa.int/ixo`

engine onto cold distant material. The analysis of large samples of high-z AGN is fundamental to understand the growth of SMBH in the centres of galaxies.

The calibration files as of December 2008 were adopted to calculate the predicted response and effective area of the IXO/WFI, Background spectra were also estimated (M. Ehle and M. Guainazzi, private communication). Here the assumed science performances of IXO correspond to those of the project [2] during 2009. In particular the effective area is 3 m^2 at 1 keV and 0.65 m^2 at 6 keV. The spectral resolution is assumed to be 150 eV for the WFI. In what follows, X-ray luminosities and intrinsic column densities N_H are in units of erg s^{-1} and cm^{-2}, respectively. Throughout this paper we have assumed a cosmological concordance model with $H_0 = 70$ km s^{-1} Mpc^{-3}, $\Omega_m = 0.3$, and $\Omega_\Lambda = 0.7$ (Spergel et al. 2003).

2 Simulations of IXO/WFI X-ray spectra

According to the AGN standard paradigm, the accretion disk around the central SMBH ($M_{BH} \approx 10^5 - 10^9$ $M_\odot$) represents an efficient mechanism for extracting gravitational potential energy and converting it into radiation, giving us the most likely explanation for the AGN engine. Strong emission in the X-ray band is probably due to a distribution of electron near the disk surface. The X-ray spectra are characterized by several components: a primary power law, a soft excess over imposed to the power law at energies below 1 keV, an iron emission line and a Compton hump. The origin of this complex spectrum is generally identified with thermal comptonization of soft photons in the optically-thick accretion disk. The Fe line (on which this work is focused) and the Compton-scattered components arise from the reflection of the X-ray emission on the disk surface or on more distant matter (Fabian & Miniutti 2005).

In particular, the Fe $K\alpha$ line, as the most prominent feature in the 6-7 keV band [3], provides an important diagnostic of the nature of the disk and the central black hole. Indeed, when the line is produced in the innermost part of the accretion disk, close enough to the SMBH, the effects of the strong gravitational field and relativistic motions may disrupt the line profile exhibiting a broad and asymmetric profile (Fabian et al. 1989; Laor 1991; Matt et al. 1992). On the other hand, if the line comes from the outer part of the accretion disk or the dust torus far from the SMBH, it displays a narrow profile. This work is focused on the narrow Fe line, ubiquitous in local AGN (Pounds

[2] See `http://ixo.gsfc.nasa.gov/science/performanceRequirements.html`

[3] The line energy depends on the ionization state. The neutral or low-ionization Fe Kα line is at 6.4 keV, while H-like or He-like Fe Kα is above 6.7 keV.

et al. 2001; Guainazzi 2003; Nandra et al. 2007) as well as is more distant AGN (Corral et al. 2008). **We further restrict ourselves to type 1 AGN, in such a way we do not need to consider a further parameter (i.e., the instrinsic absorbing column). For modestly absorbed type 2 AGN ($N_H \lesssim 10^{22}\,\mathrm{cm}^{-2}$) the flux above 2 keV is not much affected and therefore our results would apply. In fact, the equivalent width of the Fe emission line is expected to be slightly larger for Compton-thin type 2 AGN than for type 1 AGN, and even larger from Compton-thick type 2 AGN (see e.g. Bassani et al. 1999). However, for a given redshift and intrinsic X-ray luminosity this will hardly compensate the loss in counts from the source. In addition, at least some nearby Seyfert 2 galaxies (e.g., NGC 1068 Matt et al. 2004) exhibit a rather complex Fe line emission complex, making it more difficult to derive a reliable redshift, if that is a general feature of type 2 AGN.**

2.1 Simulations

The main purpose of this work is to study the possibility of obtaining the source cosmological redshift using the X-ray data, more specifically the Fe Kα emission line. For this analysis, we assume a generic X-ray spectrum for all AGN population, consisting of an absorbed power law with an emission line at the rest-frame energy of 6.4 keV. **Such narrow components have been observed with *Chandra* and *XMM-Newton* in a number of AGN (e.g. Kaspi et al. 2001; Pounds et al. 2001; Turner et al. 2002) and with a peak energy at ~ 6.4 keV and an equivalent width (EW) of $\sim 50 - 100$ eV.**

We have simulated X-ray spectra using the software package Xspec 12.5.0 (Arnaud 1996); we have included in our simulations Poisson counting noise and a spectral energy distribution due to contaminants emitting in the same band (i.e. the detector and sky backgrounds). The sky background has been obtained by averaging different regions of the sky, taking into account the column density of hydrogen in the interstellar medium ($N_H = 10^{21-22}$ cm^{-2}). M. Ehle and M.Guainazzi (private communication) **took into account several factors: (1) Non-X-ray background due to cosmic rays, (2) foreground sources, and (3) diffuse sky background due to unresolved AGN. The last one is partly introduced assuming a the $\log N/\log S$ model. This relation (number-flux relation or $N(>S)$ in the integral form) is the most fundamental measure that directly describes the contribution of individual sources to the CXB. Close to 90% of the cosmic X-ray background (CXB) is resolved in the $1-8$ keV band with current instruments, and it is foreseen that it will also be re-**

solved with medium to deep IXO exposures. These sources will then be excluded from background computations, and this is the model we have adopted here.

A set of X-ray spectral simulations, homogeneous in log L_X and z (hereafter *lx-z*) has been generated. Each cell, in the *lx-z* grid (with a step of 0.1 for log L_X and one of 0.01 for z), was simulated 100 times assuming a power law modified by Galactic absorption plus a redshifted Gaussian emission line, Xspec model: `phabs * (zpowerlaw + zgaus)`. Table 2.1 shows the parameters fixed in all simulations.

Table 1
Parameters of simulated model: `phabs * (zpowerlaw + zgaus)`

spectral component	**Parameter**	**Value**	**Comment**
Power-law	Γ	1.9	Photon index
Galactic Absorption	N_H	$2.1 \cdot 10^{20}$ cm^{-2}	Column density
Fe emission line	E_{rf}	6.4 eV	Line energy
	σ	5 eV	Line energy dispersion
	EW	100 eV	Line equivalent width

The two free parameters, normalization and redshift, are directly determined by X-ray luminosity and redshift grid. In order to be able to perform the planned spectral analysis, we considered only simulated spectra with X-ray flux in the hard $(2-10$ **keV**$)$ band greater than 10^{-15} erg cm^{-2} s^{-1} (corresponding to a S/N ratio good enough for the higher exposure time used in this work), by means of a suitable cut in the *lx-z* plane. This set of simulated spectra does not in any way mimic a true sky distribution; our only purpose is to identify the zones in the parameter space where we can measure a redshift with X-ray observations. We generate a set of approximately $200,000$ AGNs spanning a wide range of X-ray luminosities, $10^{42}-10^{46}$ erg s^{-1}, and redshifts, $z \leq 10$. The simulated process was reprised by three exposure times: one deep exposure of 1 Ms, and two moderate exposure times of 300 ks and 100 ks; these are representative of the intended multi-tiered surveys for a distant AGN with IXO.

2.2 Finding an X-ray redshift

The simulated spectra were grouped to have at least 20 counts per bin [4] and then analysed over the energy range from 0.5 keV to 10 keV. We have

[4] We adopted 20 counts as the minimum to mimic gaussian statistics from Poisson counts, which allows us to use the χ^2 minimization.

used the χ^2 statistic for the spectral analysis with the Xspec software package. Errors in estimated parameters are provided for the 90% confidence region for a single interesting parameter ($\Delta\chi^2 = 2.7$, Avni (1976)). All modelling was performed under the assumption of Galactic foreground absorption with a column density along the line of sight of $N_H = 2.1\ 10^{20}$ cm^{-2}.
The aim of this work is to quantify the Fe Kα feature. Therefore we only fitted each simulation with a single power law in the whole energy range (hereafter *baseline* model); in order to test the presence of a narrow iron line, we added to the *baseline* model a narrow Gaussian component with the energy centroid free to vary and no redshift information set.

From the measured line energy, E_o, we can obtain the redshift, defined as:

$$z = \frac{E_{rf}}{E_o} - 1 \tag{1}$$

where E_{rf} is the rest-frame emission line energy (assumed to be 6.4 keV).

To automate the analysis on the whole sample and to properly guide the fitting algorithm, we have used a trustworthy auxiliary method to generate a first guess for the value of E_o to be passed to Xspec. This method is divided into four steps:

(1) Fit the simulated spectrum with a single power law (Galactic absorption only affects low energies) to obtain the ratio between the data and this model fit;
(2) convert this ratio to Fourier space by using the discrete Fourier transform;
(3) use a low-pass filter with a cut-off frequency $\sim 17\ E^{-1}$, to remove the noise of the signal. Making an extensive test with a variety of values of this cut-off parameter, we found that the value that returns best guesses matches the instrumental spectral resolution.
(4) Finally, we must do the inverse transformation of the output of the previous step to identify the first guess for the line energy, as the peak in the filtered spectrum.

In order to statistically quantify the *best fit model* we have considered the statistic $\Delta\chi^2 \equiv \chi^2_{baseline} - \chi^2_{baseline+Gauss}$ and F-test probability value obtained from the fit of each simulation. Once the statistics $\Delta\chi^2$ and P_{F-test} have been computed, we define the discriminant $\Delta\chi^2 \geq 20$, **i.e.** 99.5% **confidence level for 2 additional degrees of freedom**, and $P_{test-F} \geq 95\%$: only fits that yield values larger than these thresholds are declared to have detected an emission line. In these cases, it will be possible to obtain the cosmological redshift. In both statistics we have also defined the efficiency of our method as the fraction of sources where we are able to detect the line (following the criteria explained above) and recover its energy with a redshift error, $\delta z \equiv$

$\Delta z/(1+z)$, of less than 5%. In the case of $\Delta\chi^2$, this can be written as

$$e(L_X, z) \equiv \frac{N((L_X, z) \quad | \quad \Delta\chi^2 > 20 \;\; \&\& \;\; \delta z < 5\%)}{N_T(L_X, z)} \tag{2}$$

and for P_{F-test},

$$e_(L_X, z) \equiv \frac{N((L_X, z) \quad | \quad P_{F-test} < 0.95 \;\; \&\& \;\; \delta z < 5\%)}{N_T(L_X, z)} \tag{3}$$

Figure 1 shows the efficiency maps of both methods ($\Delta\chi^2$ and F-test on the left and right panels respectively) for the three exposure times (one by row). Given that the IXO/WFI effective area grows towards soft X-ray energies, we did not expect constant efficiency curves (shown in colours) to coincide with constant flux contours (shown as lines). However, there are relatively sharp "transition regions" from very high (red zone) to very low (blue zone) efficiency for the three exposure times, which separate the two regions where the method is efficient and where it is not. In view of Figure 1, we conclude that this method may be used for sources with flux above these thresholds. Within the precision required, in deep exposures and at high L_X ($\sim 10^{45-46}$ erg s^{-1}) we can obtain accurate redshifts up to $z \sim 6$; and up to $z \sim 4$ and $z \sim 3$ for 300 ks and 100 ks respectively.

In order to test the reliability of our method we compared for each source the simulated redshift and the redshift obtained from the fit (Fig. 2). We see that both approaches ($\Delta\chi^2$ and P_{F-test} discrimination) provide good redshift estimates. Being the two methods similarly efficient, the $\Delta\chi^2 > 20$ discrimination is preferred, as it leaves only $< 1\%$ outliers, while the P_{F-test} discrimination can leave up to 5% outliers.

3 How many X-ray redshifts in IXO/WFI exposures

In this section, we compute the expected number of X-ray redshifts that the IXO/WFI data will deliver in realistic sky exposures, according to current AGN distribution models. For this purpose, we need to simulate redshift and X-ray luminosities for current AGN luminosity functions in the $18' \times 18'$ nominal IXO/WFI field of view. According to Figure 1, for a given exposure time, each source will have a probability for its X-ray redshift to be measurable within our specifications. Computing both quantities, $N(L_X, z)$ and $e_{\Delta\chi^2}(L_X, z)$, will tell us the number and distribution of AGNs for which

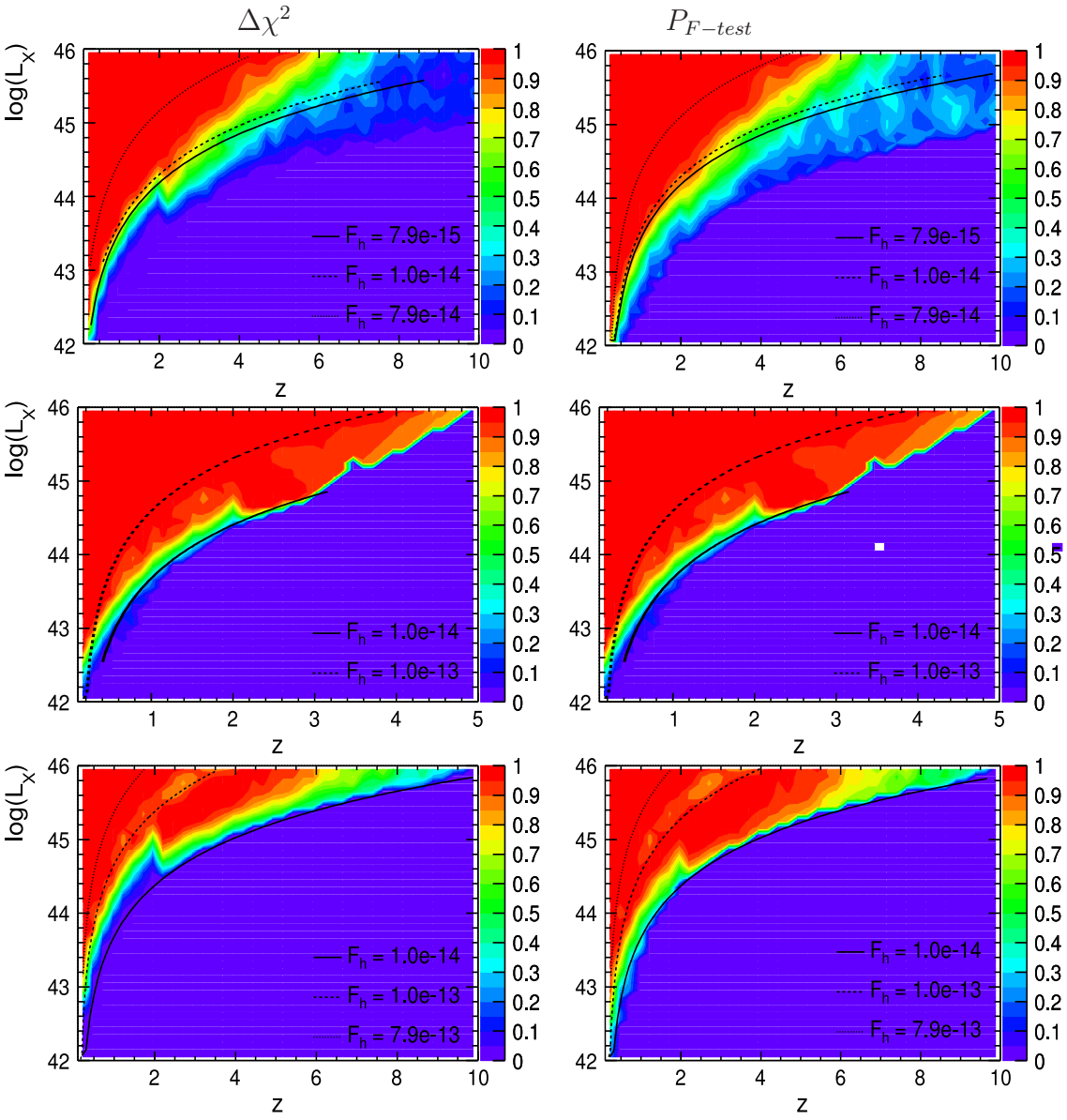

Figure 1. Efficiency maps for the three exposure times (from top to bottom): 1 Ms, 300 ks and 100 ks. *Right panels:* the efficiency maps obtained with the statistical $\Delta\chi^2$ for the three exposure times; *left panels:* the maps obtained with the F-test probability. The lines (in each map) are iso-flux lines and it can select either flux limit as a function of a limit in the efficiency.

X-ray redshifts will be obtained.

There are still large uncertainties in the exact form of the AGN evolution function; this leads to widely different estimations of the numbers of AGN that may be found at the very high redshifts probed by IXO. We have adopted the Luminosity And Density Evolution (LADE) model by Aird et al. (2010). **Although our method can reach** $z \sim 6$**, the redshifts larger than** 3

only correspond to very large luminosities and deep exposures times. Furthermore, the LADE model doesn't predict many AGN with $z > 3$; therefore in most cases, $z \sim 2-3$ would be the highest redshifts that we will be able to obtain, but this is not really constrained by the method itself, but by the paucity of more distant sources. The luminosity function of an extragalactic population, is defined as the number of objects per unit of co-moving volume per unit of logarithmic luminosity interval (Silverman et al. 2008), $d\Phi(L_X, z)/d\log L_X = dN/(dV d\log L_X)$.

The number of AGNs per unit of solid angle in a bin of X-ray luminosity $(L_X, L_X + \Delta L_X)$ and redshift $(z, z + \Delta z)$ can be written as

$$N(L_X, z) = \frac{d\Phi}{dV d\log L_X} \Delta L_X \Delta V_c \tag{4}$$

and the total number of sources per unit solid angle detected above a limiting X-ray flux (or source counts) S is given by

$$N(> S) = \int\limits_{F_X > S} dL_X \int\limits_{z=0}^{\infty} dV \, \frac{d\Phi}{dV d\log L_X} \tag{5}$$

Finally, the fraction of AGNs down to a flux S where X-ray redshifts can be obtained, is

$$\sum_{L_X} \sum_{z} \frac{e(L_X, z) \; N(L_X, z)}{N(> S)} \tag{6}$$

Figure 3 shows the number of counts in a $18' \times 18'$ field of view. In the same plot, we show the number of expected X-ray redshifts for each exposure

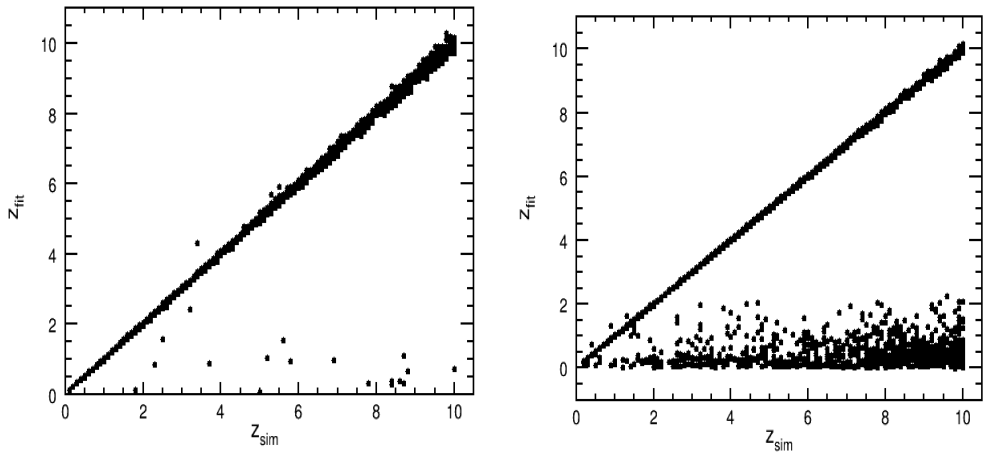

Figure 2. Fitted versus simulated redshifts. We have only included those cases in which: *(right)* $\Delta\chi^2 > 20$ and $\delta z < 5\%$; *(left)* $P_{F-test} > 95\%$ and $\delta z < 5\%$.

time as a function of the threshold flux. Simulations show that down to a reference flux of 10^{-14} erg cm^{-2} s^{-1}, X-ray redshifts can be obtained by the proposed method for 60%, 40% and 20% of AGN by IXO in an exposure time of 1 Ms, 300 ks and 100 ks, respectively.

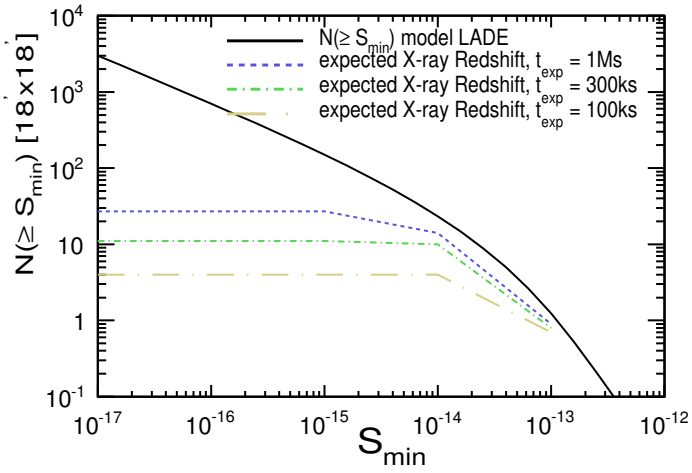

Figure 3. The number of counts in a $18' \times 18'$ field of view (solid line), and the number of expected X-ray redshifts for three exposure time: 1 Ms (dotted line); 300 ks (dash-dotted line); and 100 ks (long dash-dotted).

In Figure 4, both the expected density of AGNs according to the LADE model and the amount of AGNs with a successfully estimated X-ray redshift for 1 Ms as a function of redshift in two threshold fluxes are shown. Apart from an overall scale factor, the redshift distributions of the whole AGN population down to a flux of 10^{-14} cm^{-2} s^{-1}, and of the AGN where an X-ray redshift has been found, appear to be very similar. Moreover, in order to perform an unbinned goodness-of-fit test of this two distribution, we also used a Kolmogorov-Smirnov test (Fasano & Franceschini 1987). The most striking feature between both distributions is that it is the same distribution law with a probability above 99.5%. **Thus, with our method we can find redshifts for** 20% (50%) **of the sources down to** $2-10$ **keV fluxes of** 10^{-15} (10^{-14}) **erg cm^{-2} s^{-1}. The sources for which redshifts can be obtained are a fair sample of the total population down to these fluxes.**

It must be noted, however, that for exposure times from 1Ms down to 100ks, IXO/WFI will have a detection sensitivity of about 10^{-17} erg cm^{-2} s^{-1}. Therefore, X-ray redshifts will represent a minority of these.

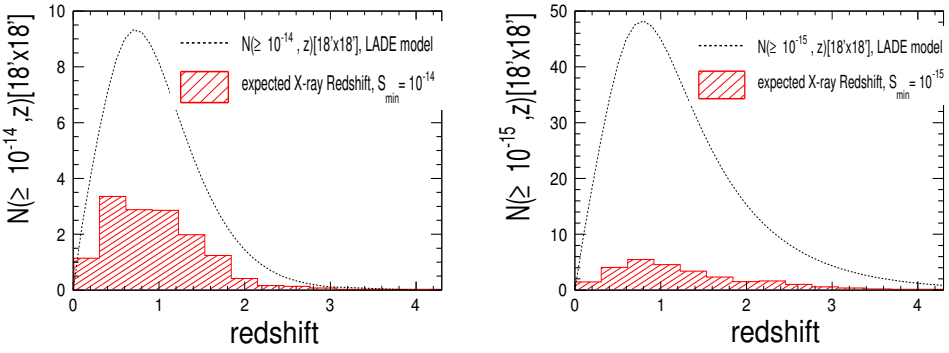

Figure 4. The histogram shows the measured X-ray redshifts fractions for 1 Ms and the dotted line displays the distribution of expected number of AGN according to the LADE model for 10^{-14} erg cm^{-2} s^{-1} (left panel) and 10^{-15} erg cm^{-2} s^{-1} (right panel) with threshold $2-10$ keV flux, respectively. **The high value of the probability ($> 90\%$) given by the Kolmogorov-Smirnov statistic tell us that both histograms are a fair representation of the total distribution of AGN.**

4 Conclusions

We have explored the capabilities of IXO/WFI to obtain AGN redshifts using X-ray data only. This is achieved by fitting the line centroid of the ~ 100 eV narrow Fe Kα emission line, ubiquitously seen in AGN. With the currently assumed IXO/WFI performances, the method successfully delivers a reliable redshift for AGN brighter than a $2-10$ keV flux of 10^{-14} erg cm^{-2} s^{-1} in 60%, 40% and 20% of the cases, for IXO/WFI exposures of 1Ms, 300ks and 100ks respectively.
Down to that flux, the redshifts sampled through this method are a fair representation of their true sky distribution.
Note added in proof. **At the time of submitting the last version of this manuscript, studies of the IXO mission have been finished by the partner agencies ESA, NASA and JAXA. Since there is no programmatic way forward for this mission, which would require a major NASA component, a more modest ESA-lead mission dubbed Athena is being studied now. Athena will likely have a WFI instrument in a focal plane, but will be fed by a smaller area. The results presented in this paper can be roughly applied to Athena, by multiplying fluxes or luminosities by the ratio of the assumed IXO effective area ($3\mathrm{m}^2$) to the corresponding area at 1 keV that Athena will end up having. Alternatively, exposure times as quoted in this paper could be enlarged by the same factor and still be applicable to Athena.**

Finally, we studied whether it would be feasible to test the reliability of the method using real data. Out of the current suite of X-ray observatories in space *XMM-Newton* is the one with the effective area closest to IXO although still much smaller ($0.4\mathrm{m}^2$ versus $3\mathrm{m}^2$). For instance, a 100 ks of exposure time for IXO corresponds to almost 1 Ms of exposure time for *XMM-Newton* even combining the data for the 3 EPIC cameras. Furthermore, its spatial resolution is also much poorer, so this raises the background and therefore reduces the sensitivity of our method. Mateos et al. (2005) detected an emission line compatible with Fe Kα in only 8 out of 123 X-ray sources detected with XMM-Newton in the Lockman Hole field with an exposure of 600 ks for the EPIC pn camera. The currently deepest XMM-Newton exposure in the Chandra Deep Field-South (totalling about 3 Ms) is currently being analyzed (Comastri et al. 2011) and it might show a number of AGN with individually detected narrow Fe emission lines.

Acknowledgements

We thank the whole IXO team for help and support and specially M.Ehle and M.Guainazzi for generating background spectra. Helpful suggestions from two anonymous referees, which resulted in significant improvement of the paper, are gratefully acknowledged. The authors thank L. Cabellos for computational support. We acknowledge partial financial support from the Spanish Ministerio de Ciencia e Innovación project AYA2009-08059. N. Castelló thanks the Spanish Ministerio de Ciencia e Innovación for a pre-doctoral fellowship. The authors acknowledge the computer resources, technical expertise and assistance provided by the Spanish Supercomputing Network (RES) node at Universidad de Cantabria.

References

Aird, J., Nandra, K., Laird, E. S., et al. 2010, MNRAS, 401, 2531

Antonelli, L. A., Vietri, M., Piro, L., et al. 2001, in Gamma-ray Bursts in the Afterglow Era, ed. E. Costa, F. Frontera, & J. Hjorth, 112–+

Arnaud, K. A., ed. 1996, Astronomical Society of the Pacific Conference Series, Vol. 101, Astronomical Data Analysis Software and Systems V

Avni, Y. 1976, ApJ, 210, 642

Bassani, L., Dadina, M., Maiolino, R., et al. 1999, ApJS, 121, 473

Blandford, R. D. & Rees, M. J., eds. 1991, Procedings of AIP Conference, Vol. 254, Testing the AGN Paradigm

Civano, F., Comastri, A., & Brusa, M. 2005, MNRAS, 358, 693
Comastri, A., Ranalli, P., Iwasawa, K., et al. 2011, A&A, 526, L9+
Comastri, A., Setti, G., Zamorani, G., & Hasinger, G. 1995, A&A, 296, 1
Corral, A., Page, M. J., Carrera, F. J., et al. 2008, A&A, 492, 71
Fabian, A. C. & Miniutti, G. 2005, ArXiv Astrophysics e-prints
Fabian, A. C., Rees, M. J., Stella, L., & White, N. E. 1989, MNRAS, 238, 729
Fasano, G. & Franceschini, A. 1987, MNRAS, 225, 155
Gebhardt, K., Bender, R., Bower, G., et al. 2000, ApJ, 539, L13
Gilli, R., Comastri, A., & Hasinger, G. 2007, A&A, 463, 79
Guainazzi, M. 2003, A&A, 401, 903
Hashimoto, Y., Barcons, X., Böhringer, H., et al. 2004, A&A, 417, 819
Hasinger, G., Miyaji, T., & Schmidt, M. 2005, A&A, 441, 417
Hopkins, P. F., Somerville, R. S., Hernquist, L., et al. 2006, ApJ, 652, 864
Kaspi, S., Brandt, W. N., Netzer, H., et al. 2001, ApJ, 554, 216
La Franca, F., Fiore, F., Comastri, A., et al. 2005, ApJ, 635, 864
Laor, A. 1991, ApJ, 376, 90
Magorrian, J., Tremaine, S., Richstone, D., et al. 1998, AJ, 115, 2285
Mateos, S., Barcons, X., Carrera, F. J., et al. 2005, A&A, 444, 79
Matt, G., Bianchi, S., Guainazzi, M., & Molendi, S. 2004, A&A, 414, 155
Matt, G., Perola, G. C., Piro, L., & Stella, L. 1992, A&A, 257, 63
Nandra, K., O'Neill, P. M., George, I. M., & Reeves, J. N. 2007, MNRAS, 382, 194
Pounds, K., Reeves, J., O'Brien, P., et al. 2001, ApJ, 559, 181
Silverman, J. D., Green, P. J., Barkhouse, W. A., et al. 2008, ApJ, 679, 118
Spergel, D. N., Verde, L., Peiris, H. V., et al. 2003, ApJS, 148, 175
Turner, T. J., Mushotzky, R. F., Yaqoob, T., et al. 2002, ApJ, 574, L123
Ueda, Y., Akiyama, M., Ohta, K., & Miyaji, T. 2003, ApJ, 598, 886